ELSEVIER

International Journal of Mass Spectrometry 203 (2000) 19–29

International Journal of Mass Spectrometry

Ab-initio-based model for the charge transfer mechanisms in $Ar^+ + H_2O$ collisions

S. Adamson[a,*], A.A. Buchachenko[a], A.I. Dement'ev[b], R.A. Dressler[c], F.X. Gadea[d], N.F. Stepanov[a], A.V. Zaitsevskii[a]

[a]*Laboratory of Molecular Structure and Quantum Mechanics, Chemical Department, M.V. Lomonosov Moscow State University, Moscow 119899, Russia*

[b]*Chair of Inorganic Chemistry, Chemical Department, Moscow State Pedagogical University, Nesvigskii per. 3, Moscow 119882, Russia*

[c]*Phillips Laboratory, Hanscom Air Force Base, Massachusetts 01731, USA*

[d]*Laboratoire de Physique Quantique, IRSAMC, Université Paul Sabatier, 118 rte de Narbonne, Toulouse cedex, France*

Received 2 August 1999; accepted 12 May 2000

Abstract

The mechanism of the charge-transfer reaction between water molecules and argon ions is analysed using a two-dimensional model with the reaction and HOH bending coordinates, which maintains the C_{2v} symmetry of the reaction system. Potential energy surfaces and nonadiabatic coupling matrix elements are computed using *ab initio* Möller-Plesset perturbation theory with multiple partitioning of the full Hamiltonian. Both *ab initio* calculations and semiclassical simulations of the vibrational distributions of the product $H_2O^+(\tilde{A})$ ion indicate two possible charge-transfer mechanisms. The first involves a nonadiabatic transition induced by radial coupling, whereas the second is governed by the curve crossing along the bending coordinate. The coexistence of two mechanisms agrees qualitatively with that inferred from the experimental measurements. (Int J Mass Spectrom 203 (2000) 19–29) © 2000 Elsevier Science B.V.

Keywords: Charge-transfer reaction; Water molecules; Argon ions

1. Introduction

Although charge-transfer (CT) mechanisms in atomic collisions are fairly well understood theoretically with the help of both analytical models and rigorous numerical calculations, an analysis of the CT processes that involve molecules still meets serious obstacles. One of the main difficulties arises when the nonadiabatic transitions are associated with the motion along internal degrees of freedom orthogonal to the scattering (or reaction) coordinate [1,2]. The mechanisms of such processes are obviously quite different from those inherent to atomic collisions, and CT dynamics cannot be described as a one-dimensional problem. This feature complicates the theoretical treatment of the dynamics as well as the electronic structure calculations requiring global multidimensional potential energy surfaces (PESs) and coupling terms.

In spite of these problems, the dynamics of several molecular CT systems were investigated in great detail at a high level of the theory {for instance, $(H + H_2)^+$ [3,5], $(H + O_2)^+$ [5,6], $(Ar + H_2)^+$ [7,8], and some others}. Most of these studies were based on the

* Corresponding author. E-mail: adamson@moleq.chem.msu.su

PII S1387-3806(00)00252-9

specific methods used in electronic structure calculations (primarily, a diatomics-in-molecule approach), which produce PESs and couplings directly in the diabatic representation. In contrast, more accurate *ab initio* electronic structure techniques are commonly based on the adiabatic representation for which the relationship to the diabatic one is not trivial in multidimensional multistate cases. In addition, rigorous dynamic calculations usually serve as benchmarks, but special efforts [8] are needed to extract from them qualitative information on the CT mechanisms that are useful for interpreting experimental data. Therefore, an analysis of the model systems associated with a particularly revealing experiment using model theoretical approaches remains important for qualitative insight in the charge-transfer dynamics of polyatomic molecules.

One particular class of CT systems may appear especially interesting in this context. Because of the importance of water in the Earth's atmosphere and in the spacecraft environment, reactions of water molecules with various atomic and molecular ions (such as N^+ [11,12], O^+ [13], Ar^+ [14,15], Kr^+ [12,16], N_2^+ [14,15], H_2O^+ [17], etc.) were thoroughly studied at hyperthermal energies using guided-ion beam and luminescence experiments. Whereas the former approach allowed the investigation of the energy dependence of reaction cross sections, the latter provided information on the product energy distribution, i.e., on the populations of near-resonant bending vibrational levels of the charge-transfer product ion H_2O^+ ($\tilde{A}$) v_2'. No evidence was observed for excitation of stretching modes, in accordance with low-ionization Franck-Condon factors. It was argued that the observed distributions and their variations with collision energy can be interpreted in terms of two coexisting charge-transfer mechanisms [12]:

(1) nonadiabatic transition along the H_2O bending coordinate θ due to collision-induced curve-crossing;
(2) nonadiabatic transition along the scattering coordinate R.

The former mechanism was suggested to be primarily operative for bending vibrational levels lying below the resonance CT energy (exothermic levels) at low-collision energies (<10 eV). The latter was thought to be responsible for the population of levels above the resonant energy (endothermic levels) at low energies, although gaining in importance for all levels as the collision energy is increased.

These findings definitely demand theoretical analysis. Although direct comparison between theory and experiment can hardly be achieved for the systems under consideration because of the large dimensionality of the problem and relatively high collision energies, simplified models can be formulated and analyzed for qualitative purposes.

In the present article, we consider the electronic structure and dynamics of the $(Ar + H_2O)^+$ charge transfer system

$$Ar^+(^2P) + H_2O(\tilde{X}^1A_1) \rightarrow Ar(^1S) + H_2O^+(\tilde{A}^2A_1) \quad (1)$$

in the frame of a two-dimensional (2D) model. Although the most telling experimental results were obtained for the N^+ and $Kr^+ + H_2O$ systems [11,12,16], we have chosen the $Ar^+ + H_2O$ system due to the simplicity of the electronic structure of the reactant ion and product neutral. A detailed comparison of the derived product state distributions for all investigated ion + H_2O systems provides evidence that for all of them the same mechanisms are operative [18].

Relevant potential energy surfaces and nonadiabatic couplings are obtained by means of *ab initio* calculations using the many-body multipartitioning perturbation theory [19,20]. This approach ensures the strict separability of the Hamiltonian with respect to the separation into $Ar^+ + H_2O$ and $Ar + H_2O^+$ fragments and describes properly the effects of dynamic electron correlation on the charge distributions [21].

2. Theory

The simplest 2D model that allows one to consider both charge-transfer mechanisms assumed for the $Ar^+ + H_2O$ collisions is illustrated in Fig. 1. The fragments move in a plane so that the C_{2v} symmetry is maintained. Both OH bond lengths ρ are held equal and fixed (at the arithmetic mean value between equilibrium distances in water and water cation, 0.979

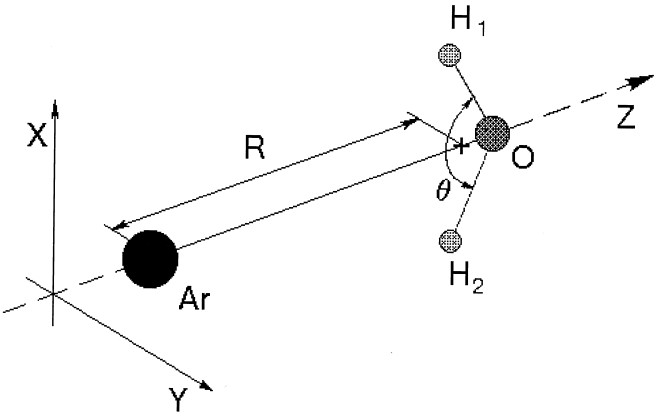

Fig. 1. Geometrical parameters of the C_{2v} model.

Å). Only two geometric parameters, the interfragment separation, R, and the HOH bending angle, θ, are allowed to vary ($\theta = 180°$ corresponds to linear molecule oriented perpendicularly to reactive coordinate R; at smallest values of θ OH bonds are directed toward the Ar atom). The choice of this model in the present study was merely dictated by its simplicity. It may be close to reality in low-energy collisions where the approaching fragments can be oriented by ion-dipole attraction (note, however, that the equilibrium geometry of the Kr^+ H_2O complex does not correspond to C_{2v} symmetry [22]).

Within the C_{2v} model, the correlation of electronic states is as follows. In the entrance channel, the unfilled p orbital of Ar^+ gives rise to states of $^2A_1$, $^2B_1$, and $^2B_2$ symmetries, whereas in the exit channel there are $^2B_1$ and $^2A_1$ states originating from the interaction of the Renner–Teller doublet of water cation with the closed-shell Ar atom. As far as no coupling between the states of the different symmetry exists, the model implies distinct charge-transfer pathways to two states of the water cation.

The total Born–Oppenheimer Hamiltonian, which describes the nuclear motion was derived using the standard technique. It has the form

$$H = -\frac{1}{2\mu}\frac{\partial^2}{\partial R^2} - \frac{1}{m_O\rho^2}\sin\theta\frac{\partial}{\partial\theta} - \frac{1}{m\rho^2}\frac{\partial^2}{\partial\theta^2} + \frac{1}{m_O\rho^2}\cos\theta\frac{\partial^2}{\partial\theta^2} + U(R,\theta) \quad (2)$$

where μ is the reduced mass of fragments, $m = m_O m_H/(m_O + m_H)$, m_O and m_H are the masses of oxygen and hydrogen nuclei; $U(R, \theta)$ is the adiabatic PES. The expressions for differential coupling operators between two electronic states i and f are

$$T_{if}^{(\theta)} = -\left\langle i\left|\frac{\partial}{\partial\theta}\right|f\right\rangle\frac{2}{m\rho^2}\frac{\partial}{\partial\theta} - \frac{2}{m_O\rho^2}\cos\theta\frac{\partial}{\partial\theta} + \frac{1}{m_O\rho^2}\sin\theta \quad (3)$$

$$T_{if}^{(R)} = -\frac{1}{\mu}\left\langle i\left|\frac{\partial}{\partial R}\right|f\right\rangle\frac{\partial}{\partial R} \quad (4)$$

where the matrix elements are taken with the adiabatic electronic wave functions.

Ab initio calculations on the adiabatic PES's and nonadiabatic coupling matrix elements were performed as follows. Contracted Gaussian basis sets $(11s7p1d)/[6s4p1d]$ for Ar, $(9s6p1d)/[4s3p1d]$ for O, and $(4s1p)/[2s1p]$ for H were obtained from the standard Dunning-Hay basis sets [23] by adding diffuse p orbitals on O (exponential parameter $\zeta = 0.059$) and polarization d orbitals on O ($\zeta = 0.8$) and Ar ($\zeta = 0.85$) centers. State-averaged complete active space multiconfigurational SCF procedure in the active orbital space spanned by two (highest occupied and lowest unoccupied) MOs ($7a_1$, $8a_1$ for the states of A_1 symmetry and $2b_1$, $3b_1$ for B_1 states) was used to generate canonical MOs. The latter were then

localized by projecting localization onto the reference SCF MOs with fractional occupancies corresponding to $(H_2O)^{+0.5} + Ar^{+0.5}$ charge distribution computed at large R and given θ. Therefore, $\ldots 7a_1^2 8a_1^1$ and $7a_1^1 8a_1^2$ configurations formed the model space for the states of A_1 symmetry, whereas $\ldots 2b_1^2 3b_1^1$ and $2b_1^1 3b_1^2$ ones for the states of B_1 symmetry. At large interfragment distances, MOs $7a_1$, $2b_1$, $8a_1$, $3b_1$ correlate with the $3p_z$, $3p_x$, $3a_1$, $1b_1$ orbitals of Ar and H_2O fragments, respectively.

The correlation effects were treated within the second-order generalized quasidegenerate Möller–Plesset perturbation theory with multiple partitioning of the total Hamiltonian (MPPT/2) [19–21]. The nonadiabatic electronic matrix elements in Eqs. (3), (4) were calculated by the finite-difference method [24,25].

3. Results

3.1. Asymptotics

The behavior of potential energy surfaces in the limit of separated fragments determines the energetics of the CT process and, owing to the availability of accurate reference data, makes it possible to characterize the quality of the present *ab initio* calculations. It is likely that such a test is representative for finite interfragment distances as well, due to size-consistency and exact separability of the MPPT/2 approach [19–21]. In particular, it has been checked that at very large interfragment distances the total energy of the system is equal to the sum of fragment energies calculated independently.

The calculated bending potential energy curves of the H_2O and H_2O^+ fragments are plotted in Fig. 2 and compared with literature data. For $H_2O(\tilde{X})$, model potential of Bunker and Landsberg [26] is presented, whereas for H_2O^+, the cuts of high-level *ab initio* multireference configuration interaction (MRCI) PESs by Brommer et al. [27] at the same OH distances ρ as chosen in this work are shown. Selected potential parameters and spectroscopic constants determined experimentally and evaluated for these one-

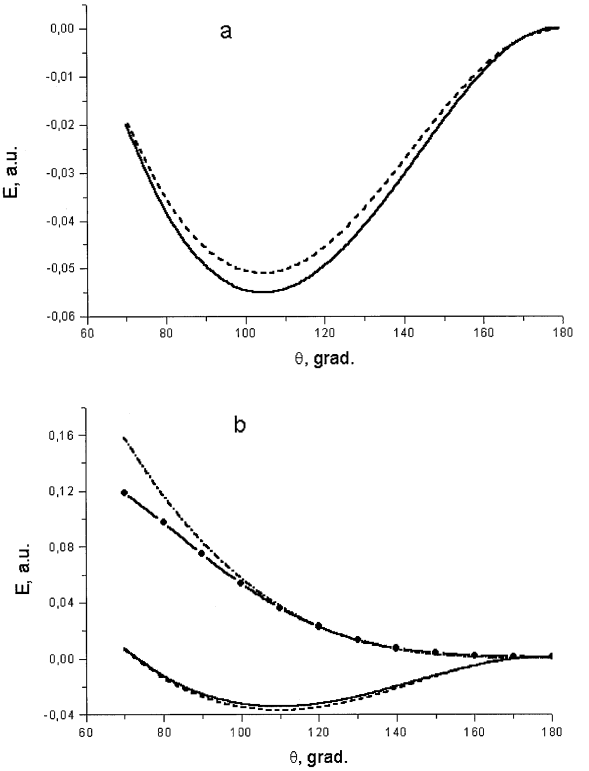

Fig. 2. (a) Potential curves for the ground state of H_2O. (-- -- --) - MPPT/2 approach; (------) data from Ref. [26]. (b) Potential curves for the ground and excited states of H_2O^+: (----) X^2A_1 and (-●-●-) A^2B_1 states, MPPT/2 approach; X^2A_1 (____) and A^2B_1 (--.--.--). Data from Reference [27].

dimensional angular potentials are listed in Table 1. A very good quality of the present results is evident, particularly in comparison with much more elaborated *ab initio* calculations from Ref. 27.

The CT process [Eq. (1)] populates highly excited bending levels v_2' of H_2O^+ ($\tilde{A}$) ion [14,15]. Table 2 compares the energies of several $\tilde{X}^2B_1$, $v_2 = 0 \rightarrow \tilde{A}^2A_1$, v_2' transitions in water cation nearby the charge-transfer resonance. Theoretical data were obtained variationally by diagonalization of the angular part of the Hamiltonian equation (2) using the basis of infinite-box functions. Calculated energies are in good agreement (~5%) with reference data, though the discrepancy increases with v_2'.

Present calculations determine a first ionization potential of Ar as 15.67 eV. This value is in good agreement with the experimental value 15.76 eV for

Table 1
Potential and spectroscopic parameters of H_2O fragments.

$H_2O(\tilde{X}^1A_1)$			
Parameter	This work	Model [26]	Exptl. [28]
ρ, Å	0.9791[a]	0.9704	0.9740
θ_e, grad	104.42	104.26	104.62
θ_0, grad[b]	105.02	104.87	105.2
$U(\theta = 180°)$, cm^{-1}	12151	13052	11470
ω_e, cm^{-1}[c]	1683(17)	1615(16)	1594
$\omega_e x_e$, cm^{-1}[c]	24.5(2.0)	20.3(2.0)	—
$H_2O^+(\tilde{X}^2B_1)$			
Parameter	This work	Model [26]	Exptl. [28]
ρ, Å	0.9791[a]	0.9791[a]	0.9988
θ_e, grad	109.7	109.6	—
θ_0, grad[b]	110.58	110.55	110.46
$U(\theta = 180°)$, cm^{-1}	8507	7850	—
ω_e, cm^{-1}[c]	1564(9)	1513(5)	1431.173
$\omega_e x_e$, cm^{-1}[c]	23.6(4.2)	20.9(2.3)	22.768
$H_2O^+(\tilde{A}^2A_1)$			
Parameter	This work	MRCI [27]	
ρ, Å	0.9791[a]	0.9791[a]	
θ_e, grad	180	180	
ω_2, cm^{-1}[d]	592(11)	589(20)	
$\frac{1}{2} h\omega_2$, cm^{-1}[d]	20.8(0.8)	19(1)	

[a] Fixed value.
[b] Vibrationally-averaged value for the ground bending state $v_2 = 0$.
[c] Obtained by fitting calculated bending spectrum to $\omega_r(v_2 + 0.5) - \omega_e x_e(v_2 + 0.5)^2$.
[d] Obtained by fitting calculated bending spectrum to $\omega_2(v_2 + 1) + \frac{1}{2} h\omega_2(v_2 + 1)^2$.

$Ar(^2P_{3/2})$ or 15.85 eV obtained by the subtraction of spin-orbit splitting [30]. A CT exothermicity for process (1) of 3.169 eV is calculated, whereas experimental data [14,31,32] are 3.14 and 3.32 eV for $Ar(^2P_{3/2})$ and $Ar(^2P_{1/2})$ reactants, respectively. The elimination of spin-orbit splitting from the experimental values yields the value 3.26 eV, which is somewhat above the current calculations. However, it was argued [14] that $Ar^+(^2P_{1/2})$ contributes little to charge transfer. Thus, our value is ~0.03 eV higher than that of the dominant $Ar^+(^2P_{3/2}) + H_2O$ CT process. Our results points to a resonance with the $v_2' = 19$ bending level in a perfect accord with experimental data [14]. (Note that the bending spectrum of $H_2O^+(\tilde{A})$ have recently been reassigned [27] and the $v_2' = 17$ level assigned to the resonant level in Ref. 14 is actually $v_2' = 19$ [12,33].)

3.2. Potential energy surfaces and coupling matrix elements

When the fragments approach each other, the two $^2B_1$ states remain essentially uncoupled and cannot lead to charge transfer. In contrast, two avoided crossings appear between the adiabatic PESs of $^2A_1$ symmetry at $R \approx 4.8$Å as seen in Fig. 3. The first avoided-crossing point at small angles (~80°) corresponds to the Ar^+ attack on the H–H side of the H_2O triangle, whereas the second one at $\theta \approx 260°$ takes place when Ar^+ approaches its oxygen vertex. The $\langle 1^2A_1|\partial/\partial R|2^2A_1\rangle$ and $\langle 1^2A_1|\partial/\partial\theta|2^2A_1\rangle$ nonadiabatic coupling matrix elements have maximum values nearby these crossing points (Figs. 4 and 5). Owing to the strong anisotropic ion-dipole interaction, the large-angle avoided crossing occurs at lower energy. It is important that at this interfragment separation the near-resonant bending levels v_2' 17 of $H_2O^+(\tilde{A})$ product ion become accessible through curve-crossing transitions.

3.3. Modeling of $H_2O^+(\tilde{A})$ vibrational distributions

The results of the *ab initio* calculations clearly indicate that charge transfer proceeds through the avoided crossings of two $^2A_1$ adiabatic PESs. According to Eqs. (2)–(4), radial and angular motions of the

Table 2
Energies of $\tilde{X}^2B_1$, $v_2 = 0 \rightarrow \tilde{A}^2A_1$, v_2' H_2O^+ transitions calculated with one-dimensional angular potentials. Experimental data from Ref. 29 for 0_{00} rotational levels have been reassigned according to the results of Ref. 27.

v_2'	This work	MRCI [27]	Exptl. [29]
7	13775.4	13008.3	13409.3
9	15795.1	14969.2	15302.5
11	17916.7	17014.4	17263.1
13	20126.4	19123.6	19272.1
15	22411.8	21280.2	21328.3
17	24760.7	23469.2	23410.2
19	27162.6	25676.6	—
21	29613.6	27886.1	—

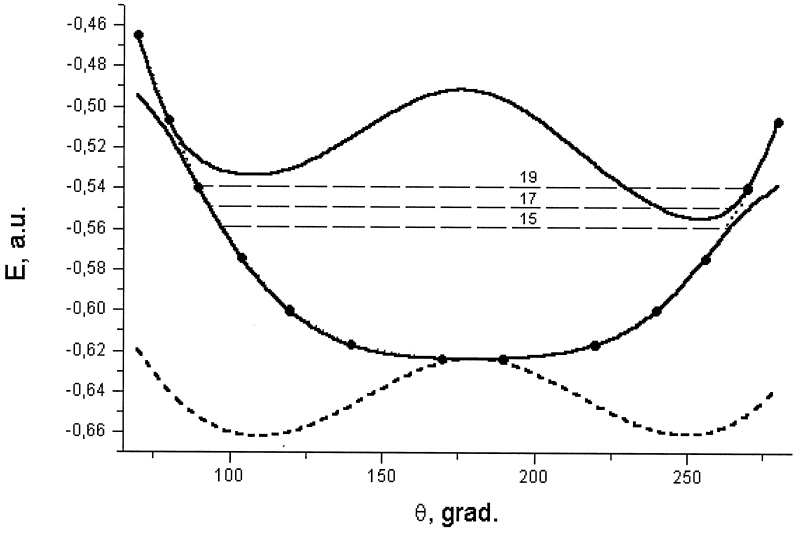

Fig. 3. Angular sections of the $1,2^2A_1$ (____) and 1^2B_1 (- - - -) PESs of $(Ar + H_2O)^+$ near the avoided-crossing region ($R = 9$ au). The 1^2A_1 (--●--) H_2O^+ PES section and vibronic levels with the $v_2' = 15, 17, 19(\tilde{A}^2A_1)$ (-- -- --) are shown.

system are coupled only by electronic terms. One can therefore separate two CT mechanisms induced by $\partial/\partial R$ and $\partial/\partial\theta$ differential nonadiabatic couplings (retaining the dependence of their electronic matrix elements on both variables).

For the qualitative treatment of the dynamical manifestations of two mechanisms, model semiclassical calculations on the distributions of product $H_2O^+(\tilde{A})$ ion over the bending levels v_2' were performed. It was these distributions and their energy dependence measured in luminescence experiments that gave rise to the hypothesis of two distinct charge-transfer pathways [12,14]. Transition probabilities were computed with the first-order classical perturbation theory [34] by the formula

$$P_\xi(v_2') = \frac{1}{\hbar}\left|\int_{-\infty}^{\infty} \langle v_2'|T^{(\xi)} \cdot[\theta, R(t)]|v_2\rangle \exp[i(\varepsilon_{v_2[\theta, R(t)]|v_2\rangle} \exp[i(\varepsilon_{v_2'} - \varepsilon_{v_2})]\, dt\right|^2 \quad (5)$$

where $\xi = R$ or θ indicates the CT mechanism, $T^{(\xi)}$ is the coupling term evaluated along the classical trajectory $R(t)$, $|v_2\rangle$ and $|v_2'\rangle$ denote bending vibrational wave functions of $H_2O(\tilde{X})$ and $H_2O^+(\tilde{A})$, respectively, and $\varepsilon_{v_2'}$, ε_{v_2} stand for the corresponding energies. Note that this semiclassical approximation does not conserve total energy.

Nonadiabatic transitions induced by angular motion were treated in an adiabatic representation so that the $T^{(\theta)}$ operator is given by Eq. (3). For numerical calculations the *ab initio* values of its electronic part $\langle\tilde{X}^2A_1|\partial/\partial\theta|\tilde{A}^2A_1\rangle$ were fitted by a Lorentzian function of θ at each value of R. The Lorentzian parameters were interpolated by splines along the R grid.

A diabatic representation was adopted for radial coupling. At each θ, adiabatic radial curves were transformed to diabatic ones using the standard two-state procedure [35]. The resulting diabatic coupling potential which stands for $T^{(R)}$ in Eq. (5) was fitted by an exponential function whose parameters were interpolated by splines over θ. Vibrational wave functions were calculated variationally for asymptotic *ab initio* angular potentials as mentioned above; the initial state of the water molecule was taken as $v_2 = 0$.

Two types of $R(t)$ trajectories were considered. The first one consisted of analytical trajectories for reference Born–Mayer or Morse potentials that were fit to the computed curves nearby the crossing points,

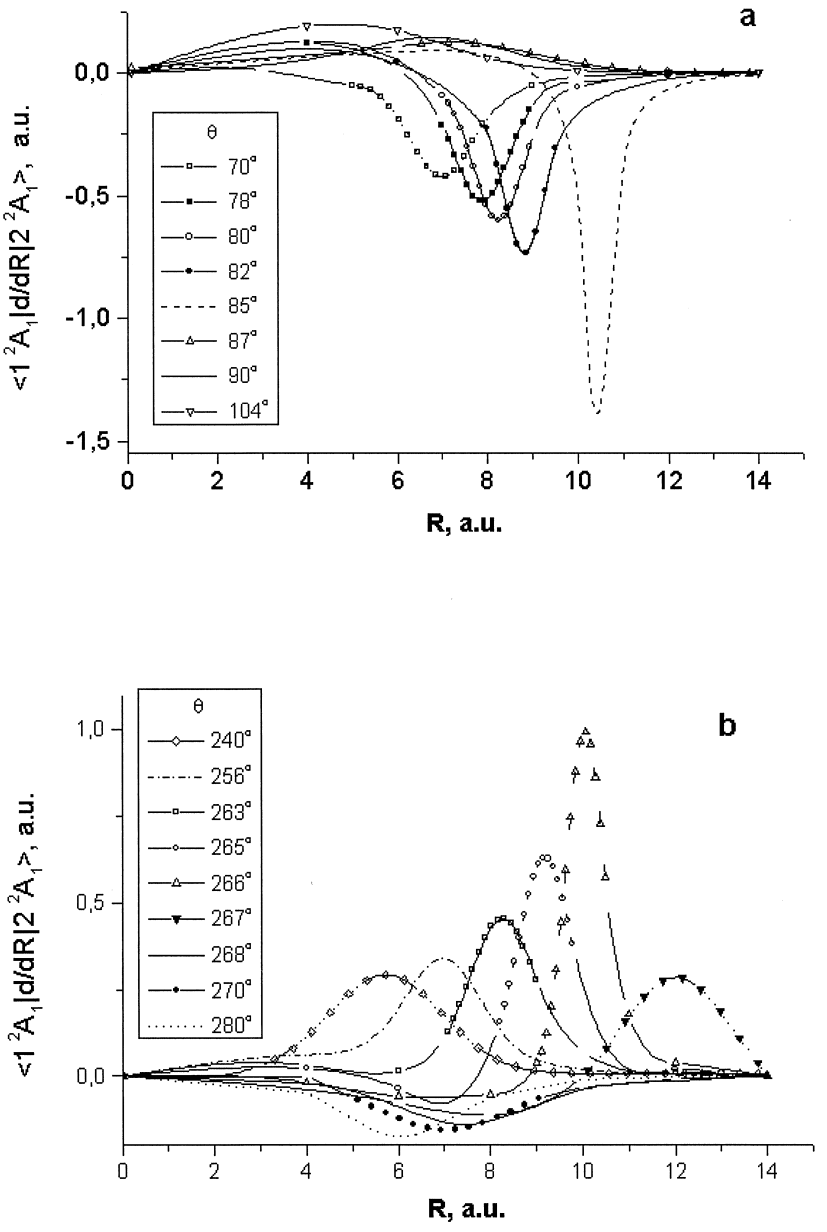

Fig. 4. $\langle 1^2A_1|\partial/\partial R|2^2A_1\rangle$ nonadiabatic coupling matrix elements at different angles θ near by small (a) and large (b) angle crossing points.

whereas the second one comprised the impact parameter trajectories $R^2(t) = b^2 + u^2t^2$, where b is the impact parameter and u is the collision velocity. No qualitative difference was found between these calculations, so we chose the second approach because it allows to calculate the vibrational state-resolved charge-transfer cross sections as

$$\sigma^{(\xi)}(v'_2) = 2\pi \int_0^\infty P^{(\xi)}(v'_2, b) b \, db \tag{6}$$

Using the impact parameter trajectories within the present 2D model implies isotropic behavior of the coupling terms. Assuming that the coupling is highest in the present C_{2v} geometry, Eq. (6) produces an

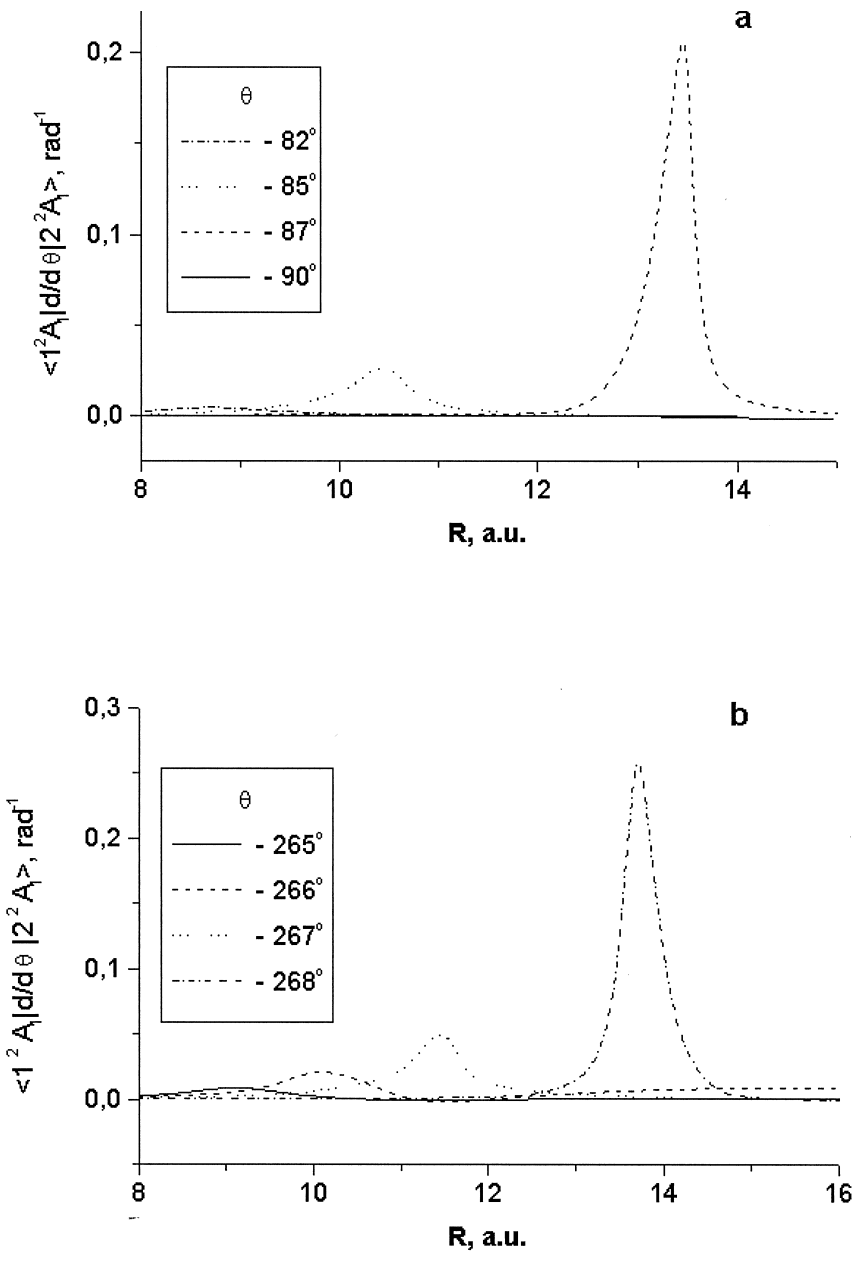

Fig. 5. $\langle 1^2A_1|\partial/\partial\theta|2^2A_1\rangle$ nonadiabatic coupling matrix elements at different angles θ near by small (a) and large (b) angle crossing points.

upper limit to the actual cross section. The absolute cross sections calculated by Eq. (6) for angular coupling for near-resonant vibrational levels are illustrated in Fig. 6. The radial mechanism exhibits very similar energy dependence of the cross sections. The calculated vibrational distributions of $H_2O^+(\tilde{A})$ ion at selected collision energies are shown in Fig. 7, which presents total populations (summed over two mechanisms) and contributions from radial and angular transitions normalized separately. The radial mechanism dominates over the angular ones, which contributes remarkably only at low collision energies. The

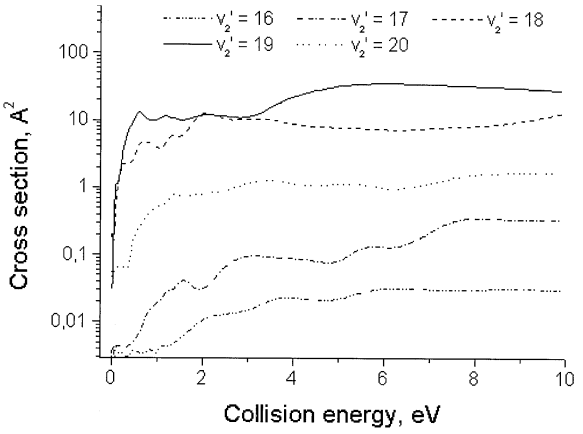

Fig. 6. Collision energy dependence of the cross sections for the formation of $H_2O^+(\tilde{A}, v_2')$ ion induced by angular nonadiabatic coupling.

radial contribution remains almost unchanged over the range of collision energies considered here and gives a strong preference to the population of the resonance $v_2' = 19$ level. Angular transitions tend to populate $v_2' = 18$ level at low energies, but with increasing energy the population maximum shifts to $v_2' = 19$ as well.

An interesting feature is the second maximum in the population induced by radial transitions at $v_2' = 17$. This can be attributed to the symmetry selection rules pertinent to C_{2v} model. At infinite interfragment separation, the reflection symmetry with respect to the $\theta = 180°$ plane orthogonal to the R axis leads to even-odd alteration of bending vibrational Franck-Condon (FC) factors $\langle v_2'|v_2\rangle$. Despite the fact that the interaction with Ar lifts this symmetry and distorts the angular potentials, even–odd v_2' alteration still manifests itself in the CT transition probabilities. It is noteworthy that in contrast to the radial coupling, the angular nonadiabatic coupling operator contains antisymmetric terms which lead to a distinct alteration pattern. It manifests itself in the calculated distributions as well (second maximum at $v_2' = 20$, see Fig. 7a). However, these effects reflect mainly the restrictions of the C_{2v} model and should be washed out if the rotations of the H_2O fragment are taken into account.

It is instructive to compare the results of the present calculations with predictions of analytical radial model suggested by Spalburg et al. [36]:

$$\sigma(v \rightarrow v') = \sigma_0 \frac{|\langle v|v'\rangle|^2}{[1 + (\Delta E/a\hbar\dot{R})^2]^3} \quad (7)$$

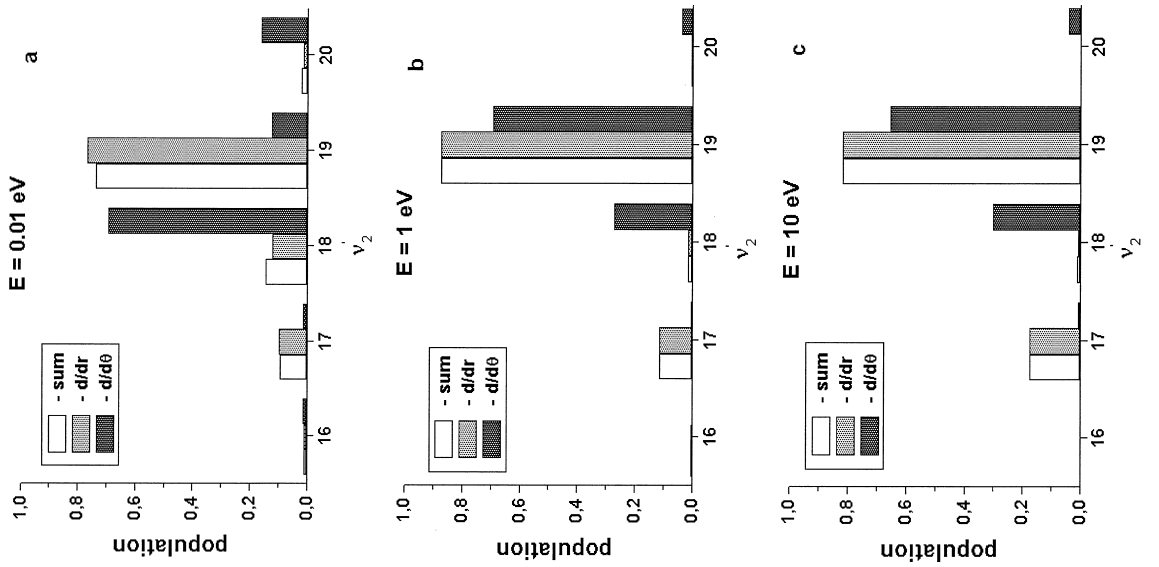

Fig. 7. Vibrational distributions of $H_2O^+(\tilde{A})$ product ion at different collision energies. Presented are the populations due to angular and radial coupling (normalized separately) and the total population calculated as the sum over both mechanisms.

where $\langle v|v' \rangle$ is an FC factor, ΔE is the energy gap between the reactant and product vibronic states and a is the parameter of an electronic coupling term $H_{12}(R)$ between electronic states 1 and 2 that has an exponential form

$$H_{12}(R) = A \exp(-aR) \quad (8)$$

According to Eq. (7), the population of product vibrational levels is governed by two factors: FC overlap with the reactant vibrational wave function and proximity to CT resonance energy. Eq. (7) predicts a preference of resonant levels with significant FC overlap at low collision energies and a Franck-Condon product state distribution at very high energies. It is worth noting that this model follows directly from Eq. (5) if one assumes that the coupling between electronic states is exponential as in Eq. (8) and does not depend on the internal coordinate θ [36]. It is therefore not surprising that the present results for radial mechanism agree well with this model.

The model of Spalburg et al. [36] can be modified to obtain a qualitative impression on the transitions induced by the angular coupling. For this purpose, the FC factors must be replaced by the matrix elements of the kinematic part of angular coupling operator (3) and a should reflect the radial behavior of its electronic part $\langle \tilde{X}^2A_1|\partial/\partial\theta|\tilde{A}^2A_1 \rangle$ shown in Fig. 5. Beyond the crossing point, the latter also drops almost exponentially, so that the calculated vibrational distributions for angular mechanism resemble those predicted by modified Eq. (7). On the other hand, the present first-order perturbation theory model (5) should be less valid for transitions induced by angular coupling where the effects of potential distortions and collision complex formation are more important.

These effects are almost certainly responsible for the differences between the present calculations and the experiments of Dressler and coworkers [12,14,15,18], where, in particular, the trend of increasing cross sections with decreasing collision energy is not reflected in the absolute state-resolved cross sections of Fig. 6 and is strongly influenced by capture collisions. In the experimental work, a predominance of exothermic levels with population maximum approximately 0.18 eV below resonance was observed at low collision energies. This was rationalized by the fact that resonance models such as Eq. (7) assume energy gaps that are independent of R. As Fig. 3 demonstrates, the potential distortions induced by the strong ion-dipole interaction in the entrance channel creates a resonance condition with exothermic $v_2' = 17$ level. The $Ar^+ + H_2O$ measurements at 12 eV exhibit a preference for $v_2' = 17$ and $v_2' = 18$ levels indicating that the transitions occur primarily at interfragment distances close to that found in the calculations (~4.8 Å). Using the realistic approximation for nonadiabatic couplings, the present first-order perturbation theory approach also neglects the effects of potential distortion on the CT dynamics. More realistic dynamics calculations are needed to get closer agreement with experimental data. They imply, however, the simultaneous description of both couplings on an equal footing. In this case the transformation from adiabatic to diabatic representations as well as the solution of the collision problem are nontrivial. More detailed calculations are the subject of future theoretical work.

4. Conclusion

The main result of the present *ab initio* calculations on the $Ar^+ + H_2O$ charge-transfer system is the demonstration of two nonadiabatic charge transfer mechanisms, one induced by the relative motion of colliding fragments and the other by the internal bending motion of the H_2O fragment. Although a two-dimensional C_{2v} model is too restrictive for allowing direct comparison with experimental data, the present results strongly support the interpretation proposed by Dressler and coworkers [12,14,15,18].

Finally, the present work is a further demonstration of the high accuracy and reliability of the efficient *ab initio* MPPT/2 approach for the calculation of potential energy surfaces and nonadiabatic couplings for ion-molecular reactions involving polyatomic molecules.

Acknowledgements

The authors are indebted to Prof. S.Y. Umanskii and Dr. S.P. Dolin for stimulating discussions. This work was supported by Russian Foundation for Basic Research project Nos. 96-03-32331, 97-03-32215 and 96-15-97469. A.A. Buchachenko and N.F. Stepanov also acknowledge the support from the Foundation Russian Universities—Fundamental research. R.A. Dressler is supported by Air Force Office of Scientific Research under Task 2303EP2.

References

[1] V. Sidis, Adv. Chem. Phys. 82 (2) (1992) 73.
[2] S. Chapman, Adv. Chem. Phys. 82 (2) (1992) 423.
[3] R.K. Pirson, J.C. Tully, J. Chem. Phys. 55 (1971) 562.
[4] C. Schlier, U. Nowotny, E. Teloy, Chem. Phys. 111 (2) (1987) 401.
[5] F.A. Gianturco, Adv. Chem. Phys. 82 (2) (1992) 135.
[6] M. Suzin, D. Grimbert, V. Sidis, M. Baer, J. Chem. Phys. 96 (1992) 307.
[7] M. Baer, Adv. Chem. Phys. 82 (2) (1992) 187.
[8] M. Suzin, F. Aguillon, V. Sidis, V. Zenevich, G.D. Billing, N. Markovic, Chem. Phys. 209 (1996) 327.
[9] H.S.W. Massey, in Applied Atomic Collision Physics, vol. 1 of Atmospheric Physics and Chemistry, Eds. H.S.W. Massey, P.R. Batles, Academic Press, New York, 1982.
[10] R.A. Dressler, E. Murad, in Unimolecular and Bimolecular Reaction Dynamics, Eds. C.-Y. Ng, T. Baer, and I. Powis, Wiley, New York, 1994.
[11] R.A. Dressler, E. Murad, J. Chem. Phys. 100 (1994) 5656.
[12] R.A. Dressler, S.T. Arnold, E. Murad, J. Chem. Phys. 103 (1995) 9989.
[13]. D.J. Levandier, R.A. Dressler, E. Murad, Chem. Phys. Lett. 251 (1996) 174.
[14] R.A. Dressler, J.A. Gardner, R.H. Salter, E. Murad, J. Chem. Phys. 96 (1992) 1062.
[15] R.A. Dressler, R.H. Salter, E. Murad, J. Chem. Phys. 99 (1993) 1159.
[16] S.T. Arnold, R.A. Dressler, M.J. Bastian, J.A. Gardner, E. Murad, J. Chem. Phys. 102 (1995) 6110.
[17] C.R. Lishawa, R.A. Dressler, J.A. Gardner, R.H. Salter, E. Murad, J. Chem. Phys. 93 (1990) 3196.
[18] R.A. Dressler, M.J. Bastian, D.J. Levandier, E. Murad, Int. J. Mass Spectrom. Ion Proc. 159 (1996) 245.
[19] A. Zaitsevskii, J.-P. Malrieu, Chem. Phys. Lett. 233 (1995) 597.
[20] A. Zaitsevskii, J.-P. Malrieu, Chem. Phys. Lett. 250 (1996) 366.
[21] S. Adamson, A. Zaitsevskii, A. Dement'ev, N.F. Stepanov, J. Phys. II (France) 7 (1997) 393.
[22] H.-S. Kim, C.-H. Kuo, M.T. Bowers, J. Chem. Phys. 93 (1990) 5594.
[23] T.H. Dunning, P.J. Hay, Mod. Theor. Chem. (Methods of Electronic Structure Theory), Ed. H.F. Shaefer III, Plenum Press, New York, 1977, p. 1–27.
[24] C. Galloy, J.C. Lorquet, J. Chem. Phys. 67 (1977) 4672.
[25] G. Hirsch, P.J. Bruna, R.J. Buenker, S.D. Peyerimhoff, Chem. Phys. 45 (1980) 335.
[26] P.R. Bunker, B.M. Landsberg, J. Mol. Spectrosc. 67 (1977) 374.
[27] M. Brommer, B. Weis, R. Follmeg, P. Rosmus, S. Carter, N.C. Handy, H.-J. Werner, P.J. Knowles, J. Chem. Phys. 98 (1993) 5222.
[28] G. Herzberg, Spectra of Polyatomic Molecules, Van Nostrand, Princeton, 1950.
[29] H. Lew, Can. J. Phys. 54 (1976) 2028.
[30] A.A. Radzig, B.M. Smirnov, Reference Data on Atoms, Molecules, and Ions, Springer, Heidelberg, 1985.
[31] R. Derai, S. Fenistein, M. Gerard-Ain, T.R. Govers, R. Marx, G. Mauclaire, C.Z. Profous, C. Sorisseau, Chem. Phys. 44 (1979) 65.
[32] J. Glosik, B. Friedrich, Z. Herman, Chem. Phys. 60 (1981) 369.
[33] R.A. Dressler, S.T. Arnold, J. Chem. Phys. 102 (1995) 3481.
[34] H.A. Rabitz, R.G. Gordon, J. Chem. Phys. 53 (1970) 1815.
[35] F.T. Smith, Phys. Rev. 179 (1969) 111.
[36] M.R. Spalburg, J. Los, E.A. Gislason, Chem. Phys. 94 (1985) 327.